JOINT EUROPEAN TORUS

JET–P(91)65

M. Olsson
and JET Team

Energy Resolution Optimization of a Two-Detector Time-of-Flight Spectrometer for D-D Neutrons

Energy Resolution Optimization of a Two-Detector Time-of-Flight Spectrometer for D-D Neutrons

M. Olsson[1] and JET Team*

JET-Joint Undertaking, Culham Science Centre, OX14 3DB, Abingdon, UK

[1]Alven Laboratory KTH, Stockholm, Sweden
** See Appendix 1*

Preprint of Paper to be submitted for publication in
Nuclear Instruments and Methods

ABSTRACT.

The energy resolution of a neutron time-of-flight spectrometer designed for diagnosing deuterium fusion plasmas has been studied and optimized using numerical methods. The spectrometer consists of two spatially separated sets of fast plastic scintillators. The first set is exposed to a collimated neutron flux from the fusion plasma. The second set, which is located outside the direct neutron flux, is used to detect elastically n(p,p')n' scattered neutrons from the first set. From the measured neutron time-of-flight, the energy spectrum of the observed neutrons is deduced. A code has been developed to simulate the neutron scattering process in the spectrometer components and to calculate the energy resolution as a function of detector geometry parameters. It is shown that it is possible to extend the size of the detectors in order to improve the detection efficiency, with a minimum degradation of the energy resolution, provided the detectors are arranged in an optimal way. The knowledge thus gained has been used at the Joint European Torus (JET) tokamak. The calculated energy resolution of the time-of-flight neutron spectrometer, which was in use at JET until1990 and has now been upgraded, is presented. The technique is not limited toD-D neutrons, but is applicable to any neutron source of sufficient strength in the MeV-range.

Contents

1 Introduction

During the last decade, large fusion experiments based on the tokamak concept for magnetic plasma confinement, like JET (Joint European Torus) in Europe and TFTR (Tokamak Fusion Test Reactor) in the USA, have produced substantial numbers of neutrons through d(d,^{3}He)n (D-D) reactions in deuterium plasmas. Various techniques have been employed to diagnose the neutron emission from the plasma [1-3]. The neutron emission rate is a measure of the fusion reaction rate in the plasma, which depends on the fuel density and velocity distribution only. The neutron energy distribution carries information on the velocity distribution of the reacting nuclei. If the deuterium fuel has a Maxwellian velocity distribution, the doppler effect yields a Gaussian neutron energy spectrum, where the width, ΔE, is a measure of the deuterium ion temeperature T_i [4],

$$\Delta E_{fwhm} \approx 82.5\sqrt{T_i} \qquad (1)$$

where ΔE and T_i are in keV and fwhm stands for full width at half maximum, which is used as a measure of spectral broadenings throughout this paper. The mean neutron energy is weakly T_i-dependent but approximately equal to 2.45 MeV. Thus, measurements of the neutron emission and energy spectrum can be used to deduce the deuterium ion density n_D and temperature T_i. Neutron spectrometry also plays an important role in discriminating neutrons of thermonuclear origin from those generated by other processes such as reactions involving fast deuterons from neutral beam injection or ion cyclotron heating of the plasma, (γ,n)-reactions and nuclear reactions involving plasma impurities, eg Be [4-7].

Essentially two different techniques for neutron spectral measurements have been employed at JET; the conventional ^{3}He-ionization chamber [8] and a time-of-flight spectrometer [9], the latter having been developed especially for JET. The main limitation of the ^{3}He-ionization chamber is that it is very sensitive to thermal and epithermal neutrons and thus easily saturates, which in practise limits the useful count-rate of D-D neutrons to about 200 counts/s. The time-of-flight spectrometer is essentially insensitive to thermal and epithermal neutrons and has a higher saturation level at the expense of a more complicated (and expensive) construction.

In order to optimize the energy resolution of the time-of-flight spectrometer, a computer code has been developed which simulates the instrument. Some experimental investigations of the instrument with a (nearly) monoenergetic neutron source at an accelerator laboratory have been made earlier [9,10]. However, the available neutron

source strength at an accelerator is much less than the neutron source strength at JET, for which the instrument is designed. Thus it is necessary to position the instrument close to the accelerator target in order to keep the measurement times reasonably low, and this makes it difficult to shield the detectors from background radiation. Therefore, numerical simulation has proved to be a much more efficient way to study the instrument. The experimental results have been valuable as a validation of the numerical model. This paper presents a numerical study of the energy resolution at 2.45 MeV as a function of various instrumental parameters and introduces some basic concepts, useful when constructing such a spectrometer. It is also shown how the efficiency can be greatly improved by using larger detectors with a minimum degradation of the energy resolution. The calculated energy resolution and detection efficiency for a time-of-flight spectrometer, which was in use at JET until 1990 and has now been upgraded, is presented as an application example. The technique is not limited to D-D neutrons but is applicable to any neutron source in the 1 - 20 MeV range of sufficient strength.

2 Description of principle

The basic geometry of the instrument is shown in fig 1 and the electronic layout is given in fig 2. For a more detailed description, see ref [9]. The neutron source is viewed through a collimator. For JET the collimator is about 2m long and has a cross-section of 12cm x 5cm. The distance from the center of the plasma to the collimator is about 17m. The neutron detectors consist of fast plastic scintillators, optically coupled to fast photomultiplier tubes (PMT): for details, see ref [9]. The first detector D_0 is exposed to the collimated neutron flux and the second detector D_1 is located some distance l' away, out of the direct neutron beam. Some of the neutrons entering the first detector are elastically scattered by protons and fly with some probability in the direction of the second detector where, again, some of them interact through elastic n(p,p')n' scattering.

The recoiling protons give rise to scintillations in the plastic, which are detected and amplified by the PMTs. The resulting anode pulses from the PMTs are fed into constant fraction discriminators (CFD), producing fast timing signals, which are used to control an electronic stopwatch and time-to-digital converter (TDC). The resulting neutron flight times are digitized and routed to a computer where they are stored and can later be displayed as time-of-flight spectra.

In this way the instrument will measure the time-of-flight of the scattered neutron, and from that, the energy of the incident neutron may be calculated through the relation

$$E_n' = E_n \cos^2\phi \qquad (2)$$

where E_n' is the energy of the scattered neutron, E_n that of the incident neutron and ϕ is the scattering angle as defined in fig 1. There is, of course, also a corresponding relation for the neutron velocities,

$$v_n' = v_n \cos\phi \qquad (3)$$

where v_n' is the velocity of the scattered neutron and v_n that of the incident neutron.

The energy resolution of the instrument depends on several parameters such as the intrinsic time resolution of the electronics, scattering angle, flight path length and uncertainties in the latter two parameters due to the finite dimensions of the active detector volumes. It also depends on the orientation of the detectors, a fact that has been used to optimize the energy resolution for large detectors, as will be shown below.

3 Numerical method

A FORTRAN code has been written which simulates the scattering and detection of neutrons in the instrument. A flow chart for the core of the code is shown in fig 3. Neutron scattering positions in the two detectors; D_0 and D_1, are sampled at random within the detector volumes and scattering probabilities, self-attenuation effects and differential cross-section for the n(p,p')n' scattering process are accounted for by calculating appropriate weight factors for the events. This also includes the attenuation effect of the Carbon present in the scintillators. For each sample, the neutron time-of-flight is computed and a Gaussian distributed perturbation corresponding to the intrinsic time resolution of the electronics is added. It is then transformed to a measured energy of the incident neutron and stored with the appropriate weight in an array. The procedure is repeated until sufficient statistics are achieved, typically 10^4 times to yield an uncertainty of $\leq 1\%$ in the calculated energy resolution. A typical result for monoenergetic 2.45 MeV neutrons is shown in fig 4. The calculated peak is analysed with respect to its fwhm, which is used as a measure of the energy resolution.

4 Basic configuration

Energy resolutions have been calculated by scanning one parameter at a time from a basic configuration. The various geometrical parameters are explained in figs 5 and 6. The reasons for the D_1 detector arrangement on a sphere and the tilting of the D_0 detector are deferred to section 6. The parameters and their values for the basic configuration are given in table 1. In the following sections these will be the parameter values used for calculations, unless otherwise specified.

Table 1

Detector parameters and their values for the basic configuration, which is used as a starting point when investigating the energy resolution as a function of these. The energy resolution for this configuration is 61.3 keV and the detection efficiency is 2.93 x 10^{-7} cm^2. The efficiency is defined as the count rate in the instrument divided by the neutron flux ($cm^{-2}s^{-1}$) at the D_0 detector.

Parameter	Explanation	Value
l	Sphere diameter	2 m
l'	Flight path length	$l\cos\phi$
ϕ	Scattering angle	30°
l_0	D_0 length	1 cm
w_0	D_0 width	1 cm
t_0	D_0 thickness	1 cm
α	D_0 tilt angle	0°
r_1	D_1 radius	1 cm
t_1	D_1 thickness	1 cm
Ω	D_1 azimuthal angle	0°

The intrinsic timing uncertainty $\Delta\tau$ (typically 1.0ns), of the electronics will also affect the energy resolution. It can be determined experimentally with the aid of a positron-electron annihilation γ-source (eg ^{22}Na) arranged so that the coincident 511 keV annihilation photons interact with the two detectors, which are sensitive also to γ-photons. The γ-photons travel at the speed of light, so the spread in γ-time-of-flight due to uncertainties in the flight path length is negligible compared to the time resolution of the detectors and electronics. If τ is the neutron time-of-flight, the contribution to the energy resolution due to $\Delta\tau$, will be

$$\frac{\Delta E}{E} = 2\frac{\Delta\tau}{\tau} = 2\frac{\Delta\tau\, v_n'}{l\cos\phi} \qquad (4)$$

where the last equality results from expressing τ in terms of the flight path length l', see table 1, and the speed of the scattered neutron v_n'.

For a 2.45 MeV neutron and the basic configuration, $\tau \approx 92$ns, which yields $\Delta E \approx 53$keV. This contribution to the instrumental width is affected by the flight path length only, and thus determines the minimum flight path length to be used for a given energy resolution. For the basic configuration, the energy resolution is 61 keV, so the main contribution to the instrumental width comes from the intrinsic time resolution of the electronics.

5 Parameter scan

In the following section, the energy resolution is presented as a function of various detector parameters. The starting point is the basic configuration and, from that, the parameters are varied, one at a time. The results are presented as polynomial approximations to the calculated data points ie

$$R(x) = \sum_{i=0}^{n} c_i x^i \quad \text{(keV)} \qquad , x_{min} \le x \le x_{max} \qquad (5)$$

where R(x) is the energy resolution as a function of the parameter x and c_i i=1,..,n are constants. The polynomial approximation is valid within 1% for $x_{min} \le x \le x_{max}$. The coefficients c_i are given in the tables below together with the parameter and x_{min} and x_{max}.

Table 2

The energy resolution as a function of various detector parameters "x" is given as polynomial approximations ie $R(x) = \sum_{i=0}^{n} c_i x^i$ *(keV). The polynomial approximation is valid within 1% for* $x_{min} \leq x \leq x_{max}$. *All parameters except "x" are those of the basic configuration in table 1, unless otherwise specified (see footnotes).*

x	x_{min}	x_{max}	c_0	c_1	c_2	c_3	c_4
l^{-1}	$0.25m^{-1}$	$2m^{-1}$	0	1.2260e+02	0	0	0
ϕ	20°	60°	9.2244e+01	-4.4711e+00	2.1650e-01	-4.4860e-03	3.6364e-05
t_0	1cm	5cm	6.0960e+01	-1.0024e+00	1.4143e+00	-8.3333e-02	0
l_0 (1)	1cm	10cm	6.1300e+01	0	0	0	0
l_0 (2)	1cm	10cm	6.0603e+01	-1.9283e-01	8.3613e-01	-3.0128e-02	0
Ω (3)	0°	45°	6.1292e+01	-1.0894e-02	2.4233e-02	-2.2253e-04	0

(1) Ω=0°, (2) Ω=30°, (3) l_0=5cm

l-scan

The first parameter to be investigated is the flight path length *l'*. This is defined in terms of the sphere diameter, which is more convenient to scan. In table 2, the energy resolution as a function of various sphere diameters is given. All other parameter values are those of the basic configuration. As the relative uncertainty in the flight path scales as $1/l'$, the relative energy resolution $\Delta E/E_0$ scales accordingly. Extending the flight path is obviously an easy way to improve the energy resolution, but at the expense of a decrease in the efficiency which scales as $1/(l')^2$.

ϕ-scan

In table 2, the energy resolution is given as a function of the scattering angle ϕ. It is fairly insensitive to ϕ up to about 35°, but increases quickly for larger angles. The relation between proton recoil energy E_p' and the neutron energy E_n and ϕ is given by

$$E_p' = E_n \sin^2\phi \qquad (6)$$

The minimum proton recoil energy which is practical to detect, with good time resolution, in the D_0 detector is ≈200 keV, which sets a lower limit of ϕ to ≈20°. A scattering angle of 30° was chosen for the basic configuration. It gives easily detected proton recoil signals in the D_0 detector.

t_0-scan

The energy resolution as a function of t_0 is given. As the relative uncertainty in flight path is increased through an increase in t_0, the energy resolution also deteriorates.

l_0-scan

As l_0 is geometrically perpendicular to the flight path and the scattering angle for a D_1 azimuthal angle Ω, equal to 0°, a moderate increase in l_0 does not affect the energy resolution. However, if one wishes to increase the efficiency of the spectrometer by introducing more D_1 detectors at the same scattering angle ϕ, one has to spread them out in the azimuthal angle Ω, which makes l_0 an important parameter. The energy resolution as a function of l_0, for $\Omega = 30°$ is given as well as the energy resolution as a function of Ω for a fixed $l_0 = 5$cm.

6 Ways of extending the detectors with a minimum loss of energy resolution

Even in large tokamaks like JET, plasma parameters affecting the neutron spectrum like T_i, are hardly constant for more than a few hundred ms. Therefore, in order to obtain sufficient statistics in such a short time, it is necessary to make the instrument as efficient as possible. The most practical and economical way to achieve this is to use as large scintillators as possible for each PMT. Secondly, one can increase the number of detectors (PMTs). Large detectors generally give a poorer energy resolution than small ones as shown above, but there are ways to minimize this problem as will be shown below.

6.1 Extended D_1

In fig 5 the D_1 detector is arranged on a sphere, so that the neutron flight path length is given by

$$l' = l\cos\phi \tag{7}$$

If this is combined with eq 3 for the speed of the scattered neutron, one sees that the neutron time-of-flight becomes independent of the scattering angle.

$$\tau = \frac{l'}{v_n'} = \frac{l}{v_n} = \text{constant} \tag{8}$$

Furthermore, this gives a simple relation between the speed of the incident neutron, the time-of-flight of the scattered neutron and the sphere diameter, which simplifies the interpretation of the time-of-flight data. The time-of-flight of the scattered neutron will in this way be the same as for a fictive, unscattered neutron travelling a distance of one sphere diameter. Thus v_n is given by

$$v_n = \frac{l}{\tau} \tag{9}$$

and from v_n, E_n is deduced. Thus the neutron scattering angle is not needed for the transformation from time-of-flight to energy and it is possible to use extended D_1 detectors.

r_1-scan

In table 3 the energy resolution as a function of D_1 detector radius r_1 is given. A large area, disc-shaped D_1 detector of course deviates from the ideal spherical shape but the D_1 radius can be rather large (15 cm) before this becomes important. Other parameters are as usual those of the basic configuration.

t_1-scan

The energy resolution as a function of D_1 thickness is also given in table 3. For the spectrometer energy resolution, this is a critical parameter of the D_1 detector.

Table 3

The energy resolution as a function of various detector parameters "x", when they are varied, one at a time, from the basic configuration, is given as polynomial approximations ie $R(x) = \sum_{i=0}^{n} c_i x^i$ *(keV). The polynomial approximation is valid within 1% for* $x_{min} \leq x \leq x_{max}$.

x	x_{min}	x_{max}	c_0	c_1	c_2	c_3	c_4
r_1	1cm	30cm	6.1572e+01	-8.3236e-02	-1.1189e-02	2.4885e-03	0
t_1	1cm	5cm	5.6680e+01	1.5024e+00	3.3607e+00	-2.4167e-01	0

6.2 Extended D_0

In fig 5, it is indicated that the D_0 detector may be tilted an angle α. The justification lies in the connection between the true neutron scattering angle and the scattering position along the "w_0" side of D_0 (D_1 is here considered to be a point detector). If a neutron is scattered towards D_1 at the far edge of D_0 (seen from D_1), it will have a larger scattering angle and thus a lower speed, than if it is scattered at the near edge. By tilting the D_0 detector, one can adjust the flight path as a function of scattering position accordingly, in order to keep the neutron time-of-flight constant.

α-scan (w_0=5cm)

To find the optimal tilt angle, α has been scanned for w_0=5cm, and the result is shown in fig 7. The energy resolution has a minimum for α=60°, and it can be shown geometrically that this minimum always occurs for twice the scattering angle ($\alpha=2\phi$).

w_0-scan

In fig 8, the energy resolution is shown as a function of w_0 for an optimally tilted as well as for a non-tilted D_0 detector. In the optimal case, w_0 can be rather large (20cm) before any significant degradation of the energy resolution will occur whereas in the non-tilted case even a w_0 of a few cm is sufficient to seriously degrade the energy resolution. This is of course for a small D_1 detector so that ϕ is well defined, but even for an

extended D_1 detector, significantly better energy resolution is obtained by tilting the D_0 detector as will be shown in the following section.

7 Energy resolution of the complete instrument

The JET neutron time-of-flight spectrometer in use until 1990 consisted of one D_0 detector and twelve D_1 detectors with parameters as shown in table 4.

Table 4

Detector parameters for the neutron time-of-flight spectrometer in use at JET until 1990. The twelve D_1 detectors were located on a constant time-of-flight sphere.

Parameter / D_1 det no	*l (m)*	ϕ (°)	Ω (°)	r_1 (cm)	t_1 (cm)
1	2	22.5	24.3	5	2.54
2	2	22.5	8.1	5	2.54
3	2	22.5	-8.1	5	2.54
4	2	22.5	-24.3	5	2.54
5	2	27.5	24.3	5	1.27
6	2	27.5	8.1	5	1.27
7	2	27.5	-8.1	5	1.27
8	2	27.5	-24.3	5	1.27
9	2	32.5	24.3	5	1.27
10	2	32.5	8.1	5	1.27
11	2	32.5	-8.1	5	1.27
12	2	32.5	-24.3	5	1.27

D_0 detector			
Parameters			
l_0 (cm)	w_0 (cm)	t_0 (cm)	α (°)
11	5	2.54	55

For this configuration, the scattering angle ϕ, is no longer well defined as the D_1 detectors cover a range of scattering angles from approximately 20° to 35°. But it is still

advantageous to tilt the D_0 detector by twice the average scattering angle. In fig 9, the result for the configuration in table 4 is shown. The energy resolution is 104 keV. For comparison, the energy resolution for the same configuration but with a non-tilted D_0 (α=0) is 125 keV. Compared to the basic configuration with detector sizes of about 1 cm, the energy resolution has deteriorated moderately from 61 keV to 104 keV but the efficiency has increased massively from 2.93 x 10^{-7} cm^2 to 1.04 x 10^{-2} cm^2, ie an increase of 3.5 x 10^4. The efficiency is defined as the count rate in the instrument divided by the neutron flux ($cm^{-2}s^{-1}$) at the D_0 detector. From eq (1), it is seen that 104 keV corresponds to a deuterium ion temeperature of 1.6 keV.

8 Conclusions

Numerical simulations have been most useful, when studying and optimizing the energy resolution of a neutron time-of-flight spectrometer for fusion plasma diagnostics. By careful arrangement of the detectors, it is possible to use large and thus more efficient detectors without unacceptable degradation of the energy resolution. Two particularly useful techniques are the "constant time-of-flight sphere" arrangement of the D_1 detectors and tilting the D_0 detector. Both of these have been used at JET. The technique is in principle applicable to any neutron source in the MeV-range.

9 Acknowledgements

The author would like to thank Dr T Elevant from the Alfvén Laboratory in Stockholm, Drs O N Jarvis, G Sadler and Mr P v Belle from JET and Dr G Grosshög from Chalmers University in Gothenburg, for fruitful discussions.

10 References

[1] H W Hendel, *Neutron Yields and Spectra from Fusion Plasmas*, in Diagnostics for Fusion Reactor Conditions, (Varenna 1982), EUR 8351-I-EN

[2] O N Jarvis, *Neutron Detection Techniques for Plasma Diagnostics*, in Diagnostics for Fusion Reactor Conditions, (Varenna 1982), EUR 8351-I-EN

[3] J D Strachan, *The Application of Fusion Reaction Product Diagnostics in Toroidal Devices*, in Diagnostics for Fusion Reactor Conditions, (Varenna 1982), EUR 8351-I-EN

[4] P v Belle and G Sadler, Basic and Advanced Diagnostic Techniques for Fusion Plasmas (Proc Course and Workshop, Varenna 1986) Vol III, EUR 10797 EN, CEC (1987) 767, and references therein.

[5] O N Jarvis et al, Nuclear Fusion, Vol 28, No 11 (1988), p 1981

[6] G Sadler and M J Loughlin, Europhysics Conference Abstracts, Vol 14B, part I, pp 1-4 (1990)

[7] M J Loughlin, P van Belle, N P Hawkes, O N Jarvis, G Sadler and D B Syme, Nuclear Instruments and Methods in Physics Research, A281 (1989) 184-191, North Holland, Amsterdam

[8] S Shalev and J M Cuttler, Nucl Sci Eng 51 (1973) 52

[9] T Elevant, D Aronsson, P van Belle, G Grosshög, M Hök, M Olsson and G Sadler, *The JET neutron time-of-flight spectrometer*, Nuclear Instruments and Methods in Physics Research A306 (1991)

[10] T Elevant, Nucl. Instr. and Meth. 185 (1981) 313

Fig 1

Detector geometry

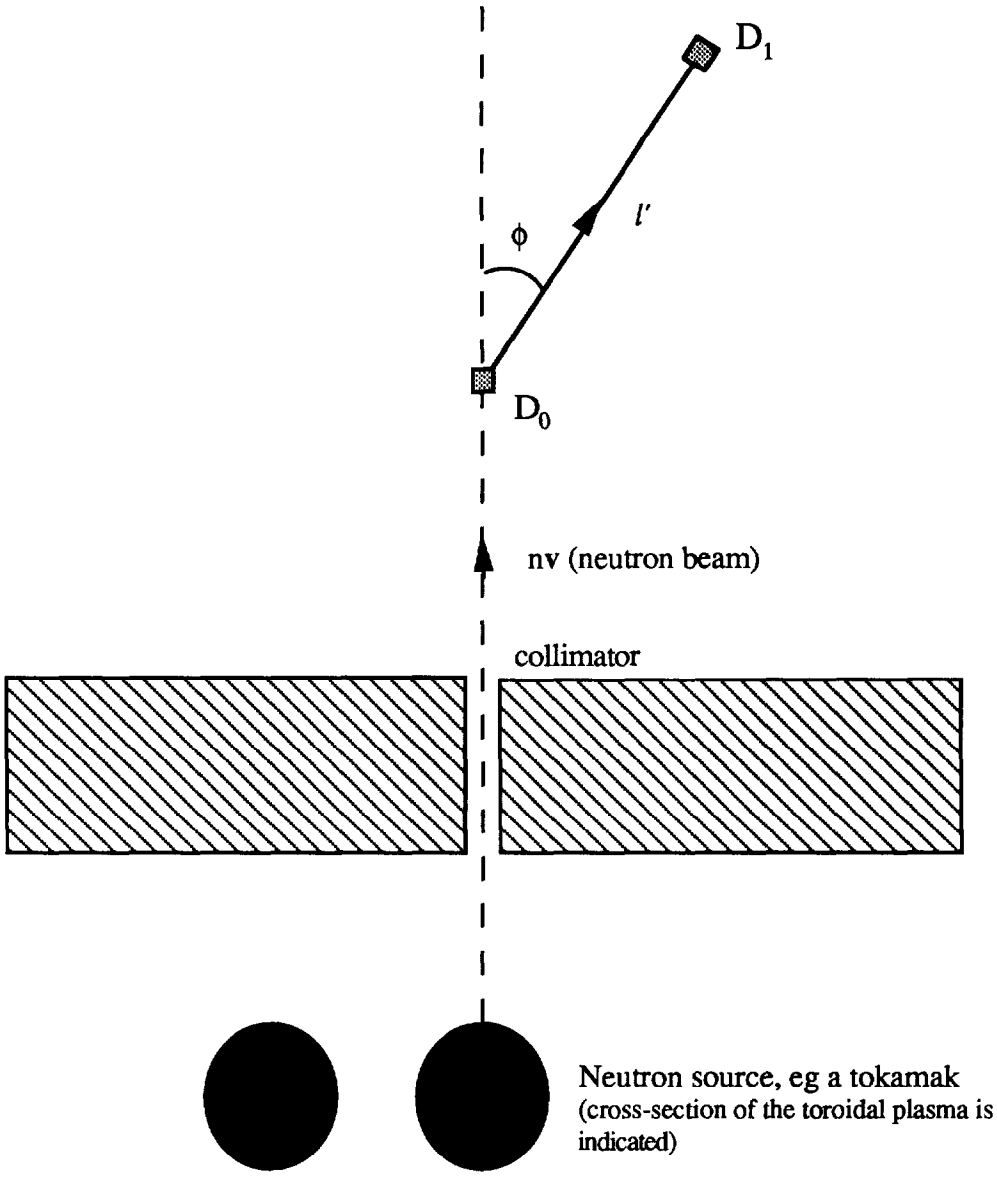

Schematic geometry of the time-of-flight spectrometer is shown. The detectors, D_0 and D_1 consist of fast plastic scintillators, optically coupled to photomultiplier tubes. Some of the neutrons are elastically scattered by hydrogen nuclei in D_0, and some of these fly towards D_1, where again some of them interact and the elapsed time-of-flight between the two interactions is measured.

Fig 2

Electronic layout
(schematic)

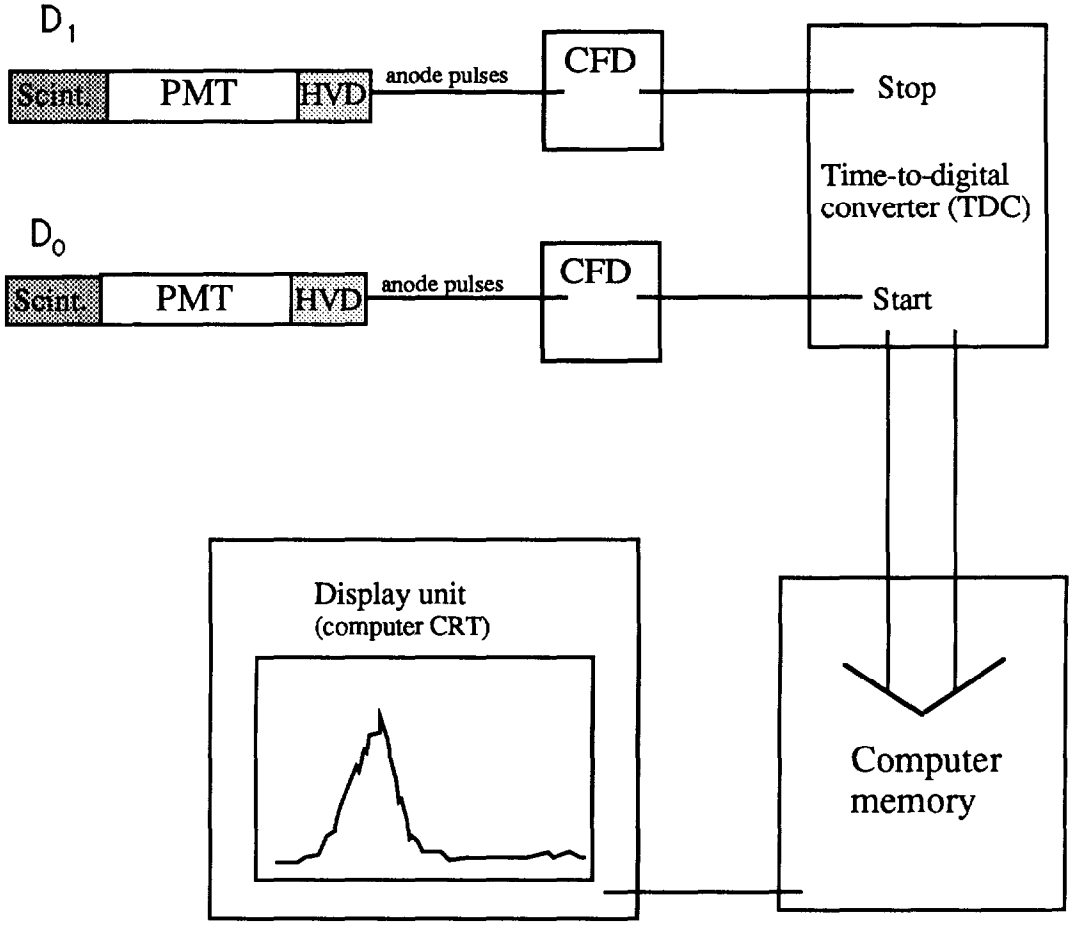

Abbreviations:

Scint. = Scintillator
PMT = Photomultiplier tube
HVD = High Voltage Divider
CFD = Constant Fraction Discriminator

A schematic layout of the signal processing chain is shown. Neutron scattering events in the detectors give rise to negative anode pulses which are processed by constant fraction discriminators (CFD), giving timing signals to the time-to-digital converter (TDC). The time between consecutive events in detectors D_0 and D_1 is measured and digitized by the TDC and routed to a memory unit. Acquired data are analysed and displayed (off-line) by a computer.

Fig 3

Flow chart

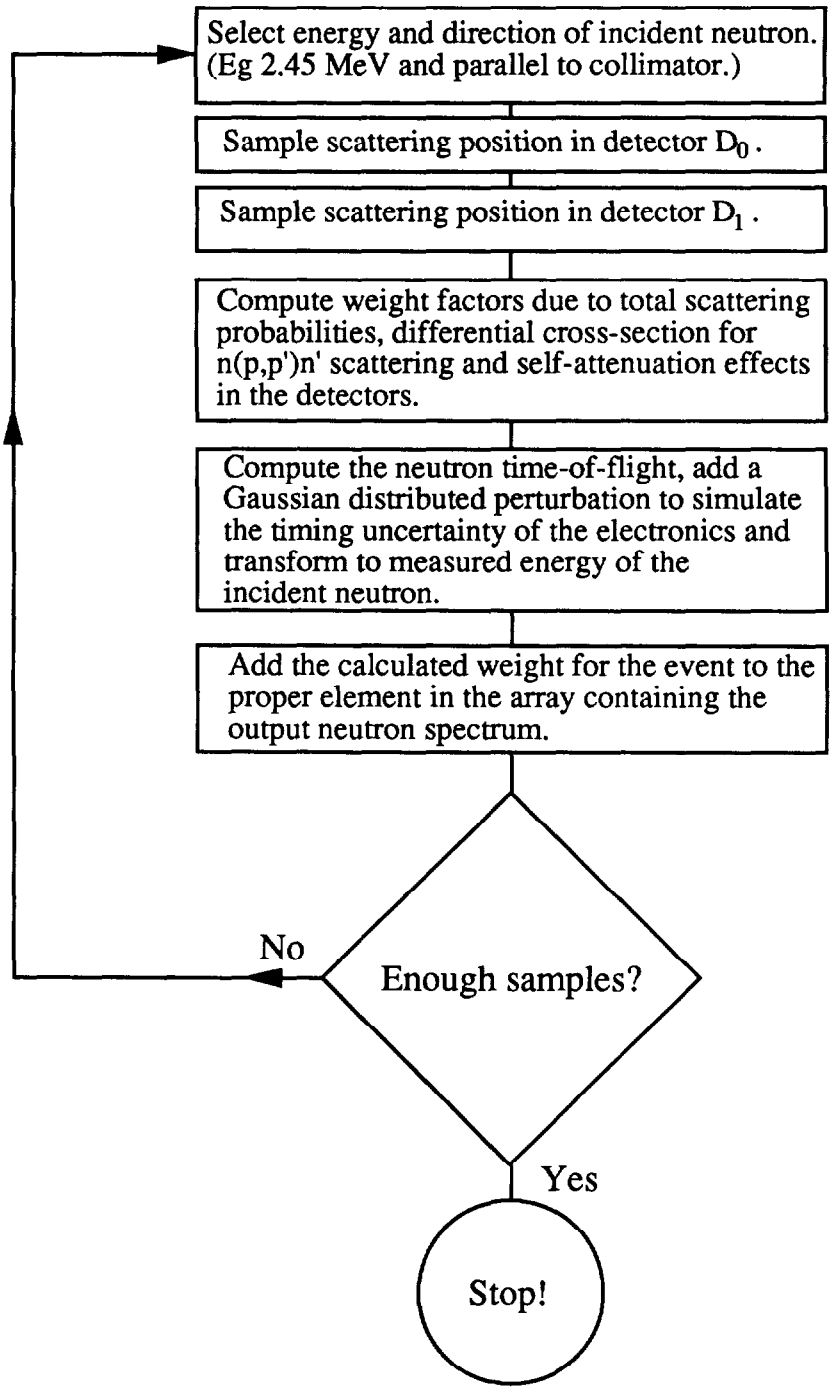

A flow chart for the core of the code, used to calculate the instrumental response to D-D neutrons, is shown.

Fig 4

Calculated spectrometer response to monoenergetic
2.45 MeV neutrons

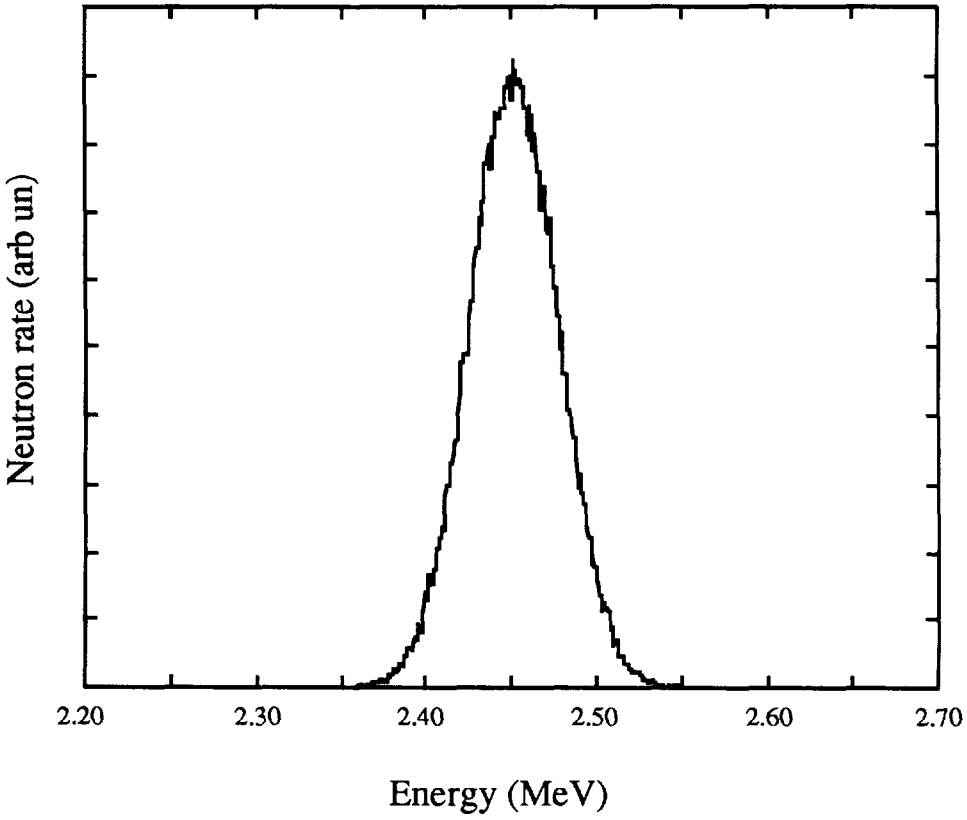

Calculated spectrometer response to 2.45 MeV monoenergetic neutrons for the basic configuration, described in table 1. The energy resolution (fwhm), is 61 keV.

Fig 5

Side elevation

(and parameters for calculations)

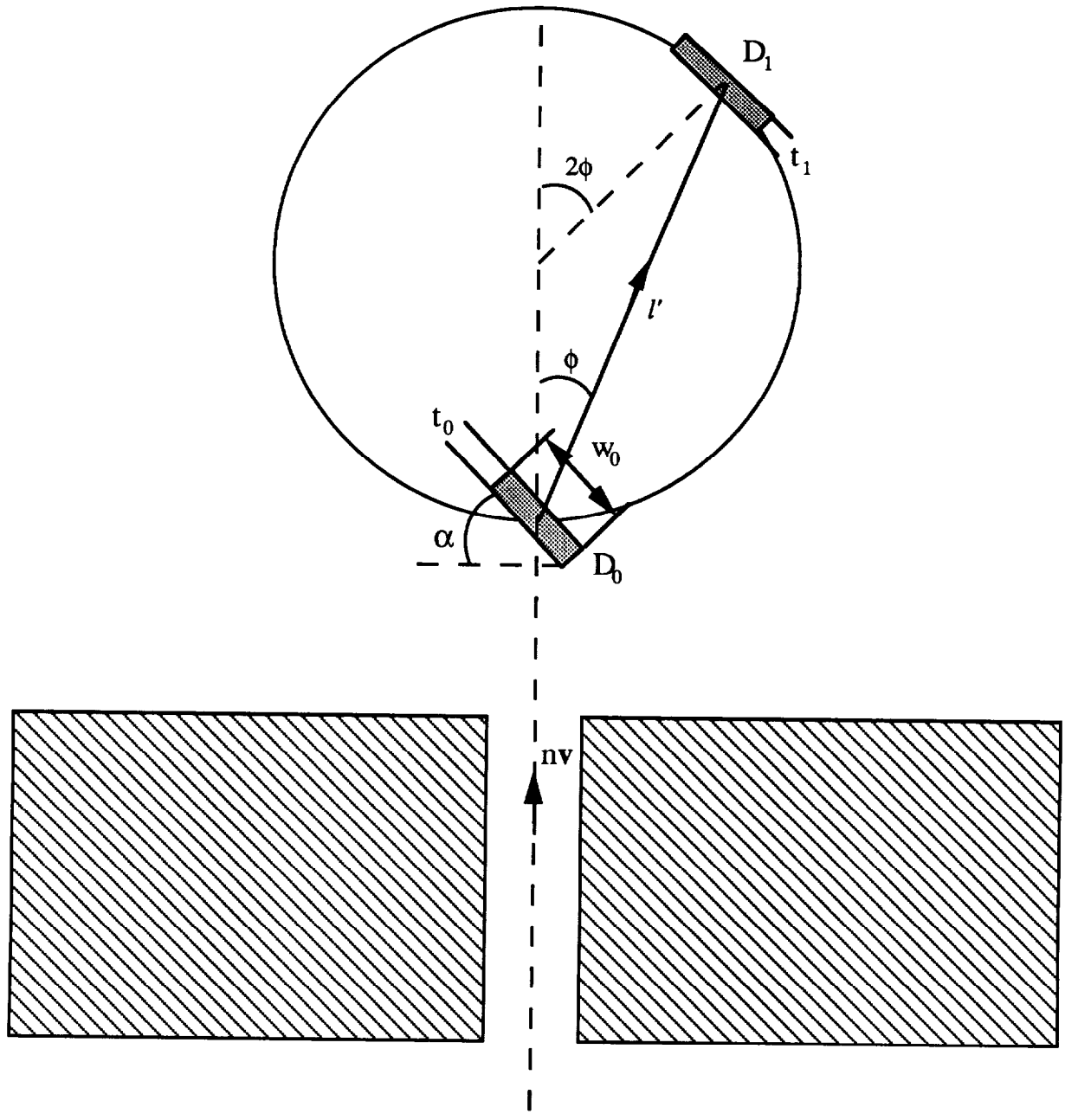

Side elevation of the spectrometer and explanation of parameters used in the calculations.

Fig 6

Plan view

(and parameters for calculations)

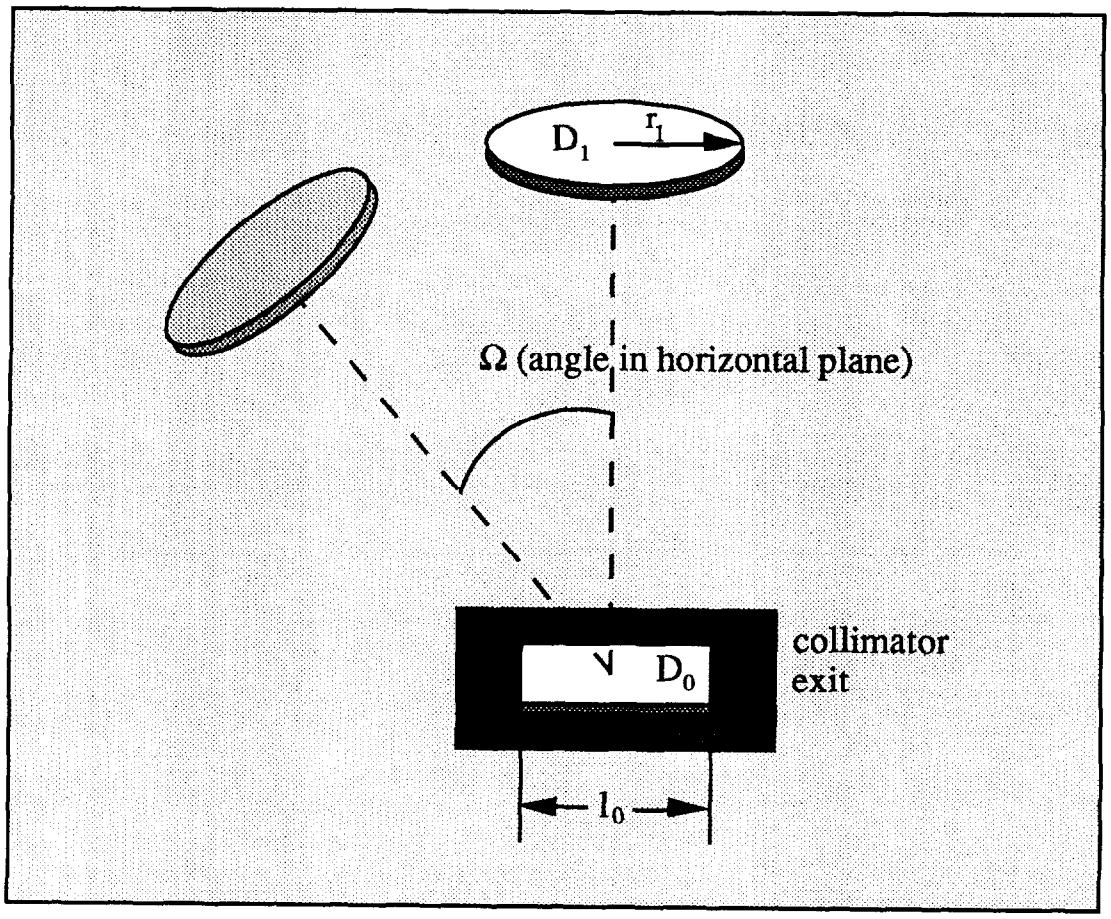

Plan view of the spectrometer and explanation of parameters used in the calculations. The possibility to increase the spectrometer efficiency by using more D_1 detectors, spread out in the azimuthal angle Ω, is indicated.

Fig 7

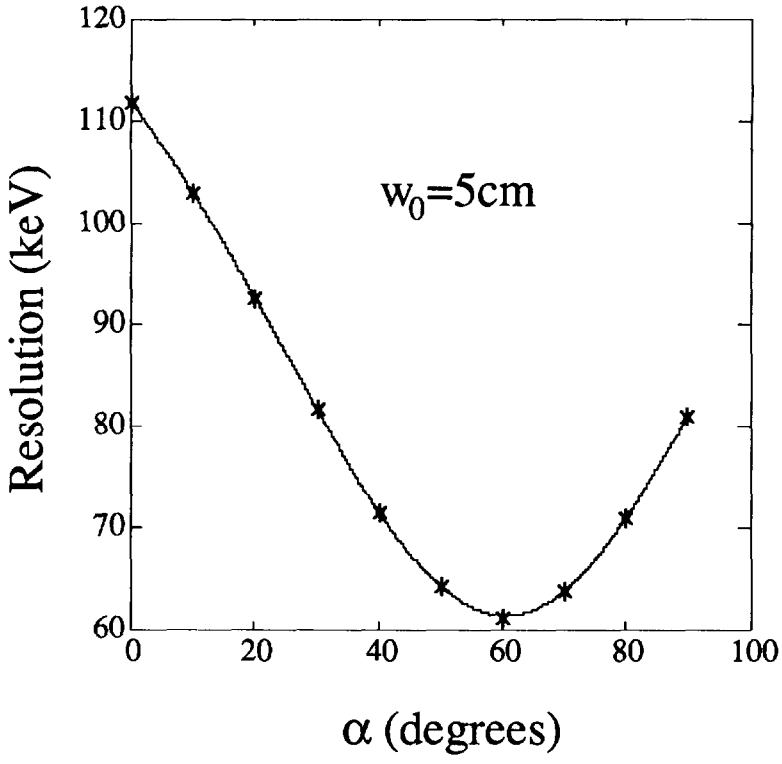

The optimization of the D_0 tilt angle α, for a D_0 width,w_0=5cm. Remaining parameter values are those of the basic configuration, see table 1. An optimum is found for α=60°. It can be shown that this optimum always occurs for twice the scattering angle (α=2ϕ).

Fig 8

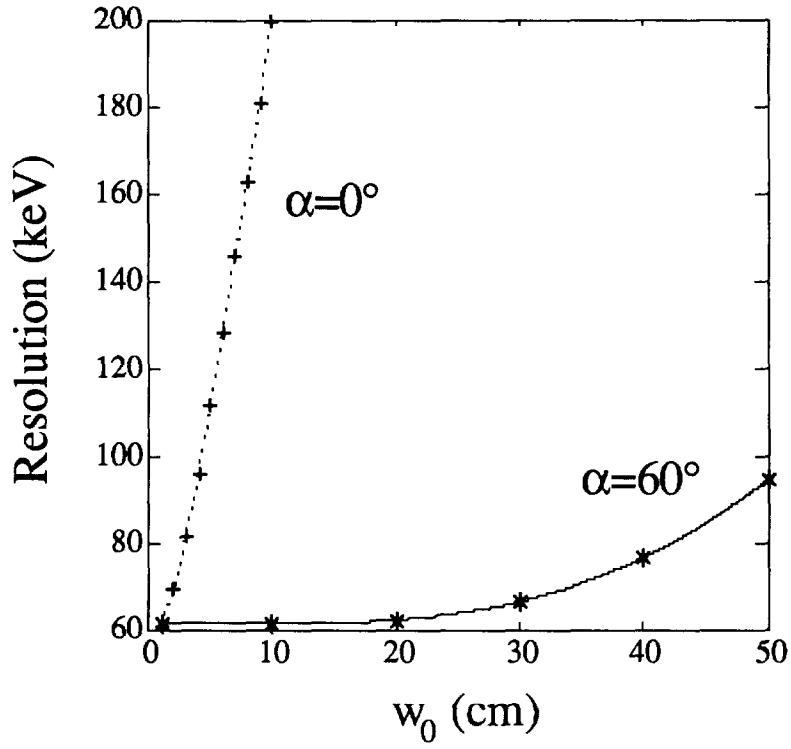

The energy resolution is shown as a function of w_0 for an optimally tilted (α=60°), as well as for a non-tilted D_0 detector. Remaining parameter values are those of the basic configuration, see table 1. Tilting the D_0 works best when the D_1 is small so that ϕ, and thus the optimal tilt angle ($\alpha=2\phi$), is well defined.

Fig 9

Calculated response to monoenergetic 2.45 MeV neutrons
for complete instrument with tilted D_0

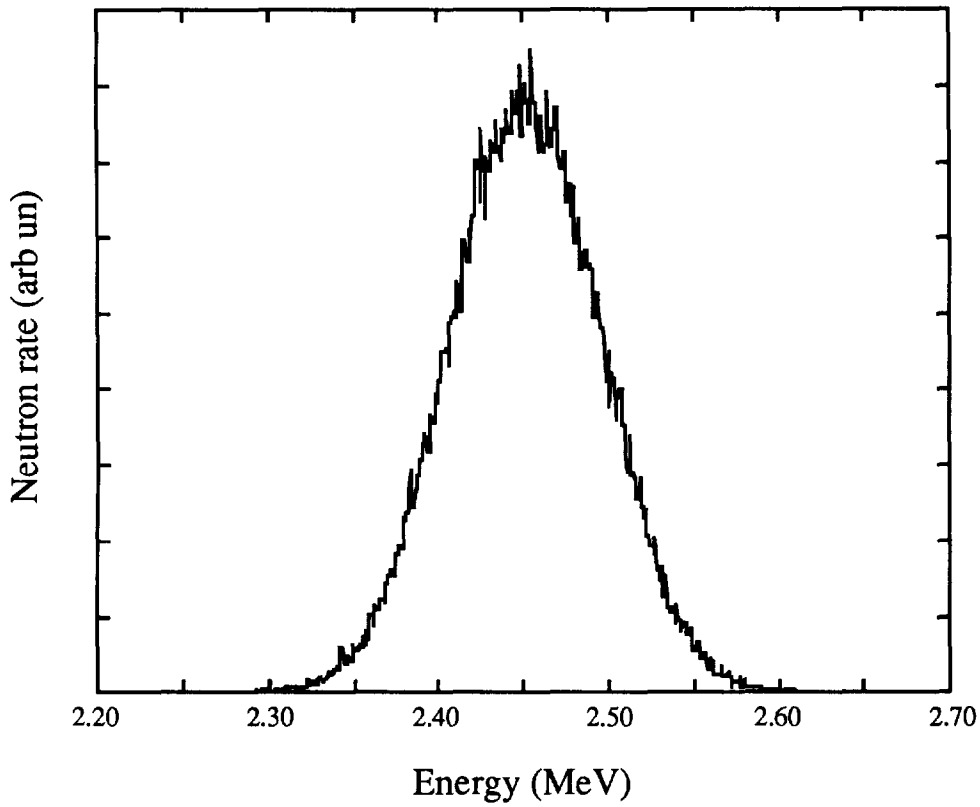

The calculated response for the JET neutron time-of-flight spectrometer is shown. Parameters for the instrument, which consists of several detectors, are given in table 4. The energy resolution is 104 keV (fwhm). For comparison, the energy resolution for the same configuration but with a non-tilted D_0 (α=0) is 125 keV. Compared to the basic configuration, the energy resolution has deteriorated moderately from 61 keV to 104 keV whereas the efficiency has increased from 2.93 x 10^{-7} cm^2 to 1.04 x 10^{-2} cm^2, ie an increase of 3.5 x 10^4. The efficiency is defined as the count rate in the instrument divided by the neutron flux ($cm^{-2}s^{-1}$) at the D_0 detector.

Appendix I

THE JET TEAM

JET Joint Undertaking, Abingdon, Oxon, OX14 3EA, U.K.

J.M. Adams[1], H. Altmann, A. Andersen[14], P. Andrew[18], M. Angelone[29], S.A. Arshad, W. Bailey, P. Ballantyne, B. Balet, P. Barabaschi, R. Barnsley[2], M. Baronian, D.V. Bartlett, A.C. Bell, I. Benfatto[5], G. Benali, H. Bergsaker[11], P. Bertoldi, E. Bertolini, V. Bhatnagar, A.J. Bickley, H. Bindslev[14], T. Bonicelli, S.J. Booth, G. Bosia, M. Botman, D. Boucher, P. Boucquey, P. Breger, H. Brelen, H. Brinkschulte, T. Brown, M. Brusati, T. Budd, M. Bures, T. Businaro, P. Butcher, H. Buttgereit, C. Caldwell-Nichols, D.J. Campbell, P. Card, G. Celentano, C.D. Challis, A.V.Chankin[23], D. Chiron, J. Christiansen, C. Christodoulopoulos, P. Chuilon, R. Claesen, S. Clement, E. Clipsham, J.P. Coad, M. Comiskey[4], S. Conroy, M. Cooke, S. Cooper, J.G. Cordey, W. Core, G. Corrigan, S. Corti, A.E. Costley, G. Cottrell, M. Cox[7], P. Cripwell, H. de Blank[15], H. de Esch, L. de Kock, E. Deksnis, G.B. Denne-Hinnov, G. Deschamps, K.J. Dietz, S.L. Dmitrenko, J. Dobbing, N. Dolgetta, S.E. Dorling, P.G. Doyle, D.F. Düchs, H. Duquenoy, A. Edwards, J. Ehrenberg, A. Ekedahl, T. Elevant[11], S.K. Erents[7], L.G. Eriksson, H. Fajemirokun[12], H. Falter, D. Flory, J. Freiling[15], C. Froger, P. Froissard, K. Fullard, M. Gadeberg, A. Galetsas, D. Gambier, M. Garribba, P. Gaze, R. Giannella, A. Gibson, R.D. Gill, A. Girard, A. Gondhalekar, C. Gormezano, N.A. Gottardi, C. Gowers, B.J. Green, R. Haange, G Haas, A. Haigh, G. Hammett[6], C.J. Hancock, P.J. Harbour, N.C. Hawkes[7], P. Haynes[7], J.L. Hemmerich, T. Hender[7], F.B. Herzog, R.F. Herzog, J. Hoekzema, J. How, M. Huart, L Hughes, T.P. Hughes[4], M. Hugon, M. Huguet, A. Hwang[7], B. Ingram, M. Irving, J. Jacquinot, H. Jaeckel, J.F. Jaeger, G. Janeschitz[13], S. Jankowicz[22], O.N. Jarvis, F. Jensen, E.M. Jones, L.P.D.F. Jones, T.T.C. Jones, J-F. Junger, E. Junique, A. Kaye, B.E. Keen, M. Keilhacker, G.J. Kelly, W. Kerner, R. Konig, A. Konstantellos, M. Kovanen[20], G. Kramer[15], P. Kupschus, R. Lässer, J.R. Last, B. Laundy, L. Lauro-Taroni, K. Lawson[7], M. Lennholm, A. Loarte, R. Lobel, P. Lomas, M. Loughlin, C. Lowry, B. Macklin, G. Maddison[7], G. Magyar, W. Mandl[13], V. Marchese, F. Marcus, J. Mart, E. Martin, R. Martin-Solis[8], P. Massmann, G. McCracken[7], P. Meriguet, P. Miele, S.F. Mills, P. Millward, R. Mohanti[17], P.L. Mondino, A. Montvai[3], S. Moriyama[28], P. Morgan, H. Morsi, G. Murphy, M. Mynarends, R. Myrnäs[16], C. Nardone, F. Nave[21], G. Newbert, M. Newman, P. Nielsen, P. Noll, W. Obert, D. O'Brien, J. O'Rourke, R. Ostrom, M. Ottaviani, M. Pain, F. Paoletti, S. Papastergiou, D. Pasini, A. Peacock, N. Peacock[7], D. Pearson[12], R. Pepe de Silva, G. Perinic, C. Perry, M. Pick, R. Pitts[7], J. Plancoulaine, J-P. Poffé, F. Porcelli, L. Porte[19], R. Prentice, S. Puppin, S. Putvinsko[23], G. Radford[9], T. Raimondi, M.C. Ramos de Andrade, P-H. Rebut, R. Reichle, E. Righi, F. Rimini, D. Robinson[7], A. Rolfe, R.T. Ross, L. Rossi, R. Russ, P. Rutter, H.C. Sack, G. Sadler, G. Saibene, J.L. Salanave, G. Sanazzaro, A. Santagiustina, R. Sartori, C. Sborchia, P. Schild, M. Schmid, G. Schmidt[6], B. Schunke, S.M. Scott, A. Sibley, R. Simonini, A.C.C. Sips, P. Smeulders, R. Stankiewicz[27], M. Stamp, P. Stangeby[18], D.F. Start, C.A. Steed, D. Stork, P.E. Stott, T.E. Stringer, P. Stubberfield, D. Summers, H. Summers[19], L. Svensson, J.A. Tagle[21], A. Tanga, A. Taroni, A. Tesini, P.R. Thomas, E. Thompson, K. Thomsen, J.M. Todd, P. Trevalion, B. Tubbing, F. Tibone, E. Usselmann, H. van der Beken, G. Vlases, M. von Hellermann, T. Wade, C. Walker, R. Walton[6], D. Ward, M.L. Watkins, M.J. Watson, S. Weber[10], J. Wesson, T.J. Wijnands, J. Wilks, D. Wilson, T. Winkel, R. Wolf, B. Wolle[24], D. Wong, C. Woodward, Y. Wu[25], M. Wykes, I.D. Young, L. Zannelli, Y. Zhu[26], W. Zwingmann.

PERMANENT ADDRESSES

1. UKAEA, Harwell, Didcot, Oxon, UK.
2. University of Leicester, Leicester, UK.
3. Central Research Institute for Physics, Academy of Sciences, Budapest, Hungary.
4. University of Essex, Colchester, UK.
5. ENEA-CNR, Padova, Italy.
6. Princeton Plasma Physics Laboratory, New Jersey, USA.
7. UKAEA Culham Laboratory, Abingdon, Oxon, UK.
8. Universidad Complutense de Madrid, Spain.
9. Institute of Mathematics, University of Oxford, UK.
10. Freien Universität, Berlin, F.R.G.
11. Swedish Energy Research Commission, S-10072 Stockholm, Sweden.
12. Imperial College of Science and Technology, University of London, UK.
13. Max Planck Institut für Plasmaphysik, Garching bei München, FRG.
14. Risø National Laboratory, Denmark.
15. FOM Instituut voor Plasmafysica, 3430 Be Nieuwegein, The Netherlands.
16. University of Lund, Sweden.
17. North Carolina State University, Raleigh, NC, USA
18. Institute for Aerospace Studies, University of Toronto, Downsview, Ontario, Canada.
19. University of Strathclyde, 107 Rottenrow, Glasgow, UK.
20. Nuclear Engineering Laboratory, Lapeenranta University, Finland.
21. CIEMAT, Madrid, Spain.
22. Institute for Nuclear Studies, Otwock-Swierk, Poland.
23. Kurchatov Institute of Atomic Energy, Moscow, USSR
24. University of Heidelberg, Heidelberg, FRG.
25. Institute for Mechanics, Academia Sinica, Beijing, P.R. China.
26. Southwestern University of Physics, Leshan, P.R. China.
27. RCC Cyfronet, Otwock Swierk, Poland.
28. JAERI, Naka Fusion Research Establishment, Ibaraki, Japan.
29. ENEA, Frascati, Italy.

At 1st June 1991